Materials Research. 2020; 23(5): e20200296
DOI: https://doi.org/10.1590/1980-5373-MR-2020-0296

Effect of MoS_2 Concentration on Microstructure and Tribological Behavior of Electrophoretic-Electrodeposited Ni-Co-Al_2O_3-MoS_2 Composites

Ya-gang Zhang[a], *Wan-chang Sun*[a]*, *Min Ma*[a], *Sha-sha Tian*[a], *Yu-wan Liu*[a], *Yan Xiao*[a]

[a] *Xi'an University of Science and Technology, College of Materials Science and Engineering, Xi'an, Shaanxi 710054, China*

Received: July 06, 2020; Revised: August 25, 2020; Accepted: September 02, 2020

Ni-Co-Al_2O_3-MoS_2 composite coatings were prepared on the surface of LY12 aluminum alloys by electrophoresis-electrodeposition with different MoS_2 concentrations. The microstructure, morphologies and composition of Ni-Co-Al_2O_3-MoS_2 composites were characterized by X-ray diffractometer (XRD) and scanning electron microscopy (SEM) equipped with energy dispersive spectroscope (EDS). The micro-indentation hardness as well as friction and tribological properties of the coatings were tested by micro-hardness tester and friction and wear tester separately. Results revealed that the composite coating fabricated at 1.0 g·L^{-1} MoS_2 achieved dense structure, and the average thickness of the coating was 39.820 μm. The micro-indentation hardness of the composite coating was decreased from 578 HV to 465 HV with the increase of MoS_2 concentration. Also, the composite coating synthesized at 1.0 g·L^{-1} MoS_2 had the lowest friction coefficient and wear rate.

Keywords: *Ni-Co matrix, Molybdenum sulfide, Alumina, Microstructure, Anti-friction characteristics.*

1. Introduction

Aluminum alloy, with numerous advantages such as light weight and excellent mechanical strength, has been widely used in aerospace, automobile, machinery manufacturing, shipbuilding and chemical industry. However, the poor hardness and wear resistance of aluminum alloy are the bottleneck of its wide application, so improving its mechanical properties has always been a research hotspot[1-5].

Electrophoresis-electrodeposition technology[6,7], which can embed various particles such as Al_2O_3[8], MoS_2[9], TiC[10], TiO_2[11], ZnO[12], ZrO_2[13] and SiC[14] into metal or alloy matrix to form cermet composite coating with excellent mechanical and electrochemical performance, has drawn great attention. Among the numerous embeddable particles, MoS_2 with layered structure is an ideal solid lubricant for the preparation of coatings with excellent friction and wear resistance[15]. The introduction of solid lubricant can obviously improve the wear resistance of the material, thus prolonging the service life of the material[16-18]. Furthermore, Ni-Co matrix has aroused growing interest due to its exceptional comprehensive properties[19-22]. Ma et al.[23] presented the influence of the duty cycle and frequency on the microstructures and properties of SiC reinforced Ni-Co matrix nanocoating, and it is proposed that the composite coating has high hardness and excellent wear resistance under the optimized parameters. Li and Zhang[24] prepared ZrO_2 doped Ni-Co matrix composite coating by one-step DC electrodeposition process. The results show that the Ni-Co-ZrO_2 composite coating has excellent mechanical properties and corrosion resistance.

Based on our previous research and a large number of literatures[25,26], it is shown that the mechanical properties of the composite coating can be effectively improved by adding Al_2O_3 to Ni-Co alloy or adding two kinds of ceramic particles (Al_2O_3 and MoS_2) to Ni matrix. However, there are few studies on embedment Al_2O_3 and MoS_2 particles into Ni-Co alloy by a low energy consumption and high efficiency liquid deposition technology and expect to obtain new or excellent anti-friction and wear resistance. Therefore, we try to prepare Al_2O_3 and MoS_2 particle reinforced Ni-Co matrix composites with the required properties by the above methods, and evaluate its microstructure, friction and wear behavior.

In this work, we aimed to prepare Ni-Co-Al_2O_3-MoS_2 composites on the surface of LY12 aluminum alloys by electrophoresis-electrodeposition method. The effects of MoS_2 concentration in EPD bath on microstructure, micro-hardness and tribological properties (involving friction coefficient, wear rate and worn scars of the coatings) were comparatively investigated.

2. Experimental Details

2.1 Pretreatments

The substrates, LY12 aluminum alloy, were cut into size of 15 mm×15 mm×10 mm samples. The chemical compositions of the substrate are listed in Table 1. The average particle sizes of alumina (α-Al_2O_3, 99.99% in purity, ST-NANO, China) and molybdenum sulfide (99.99% in purity, ST-NANO, China) are 150 nm and 200 nm, respectively. The substrates were polished with SiC paper, and then washed in alkaline solution composed of 50 g·L^{-1} sodium hydroxide, 10 g·L^{-1} triphosphate and 30 g·L^{-1} sodium silicate to remove surface oil contamination. The samples were immersed

*e-mail: sunwanchang@tsinghua.org.cn

Table 1. Chemical composition of LY12 aluminium alloys.

Composition (wt%)	Si	Fe	Cu	Mn	Mg	Cr	Ni	Zn	Ti	Al
	0.5	0.5	3.8-4.9	0-0.9	1.2-1.8	0.10	0.50	0.25	0.15	rest

in 25% sulfuric acid medium to eliminate the oxide film. After each step, the substrates were rinsed with distilled water to avoid contamination of the pretreatment solution.

2.2 Electrophoresis-electrodeposition progress

To electrophoretic deposition Al_2O_3 and MoS_2, ethanol was acted as the dispersant according to our initial exploration. The electrophoresis was implemented in an EPD bath containing 10 g·L^{-1} alumina, 0-2.0 g·L^{-1} molybdenum disulfide, 0.5 g·L^{-1} hydrated magnesium chloride. The voltage, temperature and time of electrophoresis were kept at 80 V, 65 °C and 5 min, respectively. The chemicals used in the experiment are analytical grade. After electrophoresis, Ni-Co alloy was deposited on the sample surface by pulse electrodeposition. The pulse electroplating solution consists of 300 g·L^{-1} nickel sulfate, 60 g·L^{-1} nickel chloride and 30 g·L^{-1} cobalt sulfate. And the voltage, PH, stirring speed, temperature and electrodeposition time were kept at 1.72 V, 3-6, 350 rpm, 50 °C and 50 min, respectively. The schematic of pulse-electrodeposition process is shown in Figure 1.

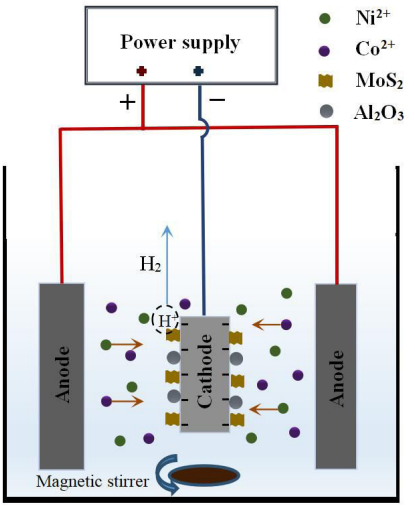

Figure 1. Schematic of the pulse-electrodeposition setup.

2.3 Characterizations

The surface and cross-section morphologies of as-fabricated Ni-Co-Al_2O_3-MoS_2 composites were viewed by SEM (JSM-6390A, Janpan). The crystalline structure of the coating was estimated by XRD (XRD-7000, Japan) with Cu Kα filtered radiation (λ=1.54 Å) generated at 40 kV and 30 mA, and the affiliated EDS was used to determine the composition of the composite coating. The micro-indentation hardness of the coating surface was measured by micro Vickers hardness tester (EM-1500L, China) for 5 s under a load of 10 N. The distance between test points is 40 μm, and the final micro-indentation hardness is the average of five measurements. The wear resistance of the composite coating was investigated under dry sliding conditions in air at room temperature by the ball-on-disk method, using a high-temperature friction and wear tester (HT-1000, China). The test was performed with a disc speed of 560 rpm and a track radius of 5 mm, using a bearing GCr15 ball (6 mm in diameter) under a load of 5 N for 10 minutes. The test is compatible with ASTM G99. Each sample was tested three times under the same conditions, and the average value was selected as the final value. The worn surface of the sample was wiped with alcohol and the wear morphologies of the coating were observed by SEM. Adhesion tester characterizing bonding strength was carried out with a load of 0.1 N and a speed of 5 mm/min.

3. Results and Discussion

3.1 Morphologies and composition

Figure 2 exhibits the cross-section and surface morphologies of Ni-Co-Al_2O_3-MoS_2 composites synthesized at 1.0 g·L^{-1} MoS_2. From Figure 2a, the dark gray area on the left is the aluminum alloy substrate, the thin gray layer in the middle area is flash-plated Ni-Co layer to prevent the substrate from corrosion in EPD bath, and the gray region on the right is Ni-Co-Al_2O_3-MoS_2 composite coating. The surface morphology of the composite coating is shown in Figure 2b, and it can be seen that the coating surface presents a mushroom-like structure. This phenomenon can be attributed to the preferential reduction of Ni^{2+} and Co^{2+} on MoS_2 particles with good conductivity or the convex regions of as-deposited metal matrix[27]. The magnified image of cross-section morphology and the EDS spectrum of as-fabricated Ni-Co-Al_2O_3-MoS_2 composites are exhibited in Figure 2c and d, respectively. It is proved that the Ni-Co-Al_2O_3-MoS_2 composite coating was well synthesized on the aluminum alloy substrate, there are no obvious cracks and delamination at the interface, and the deposited particles are homogeneously dispersed in the Ni-Co matrix without obvious agglomeration.

The energy spectra of Ni-Co-Al_2O_3-MoS_2 composites are shown in Figure 3. Obviously, there are two kinds of different particles (Al_2O_3 and MoS_2) in the composite coating. Figure 3b, c and d show the energy spectrum analysis of different regions. Results show that the light gray continuous region is Ni-Co matrix. The uniformly distributed black particles are Al_2O_3 particles and the light gray stripe particles are MoS_2 particles.

Figure 4 represents the XRD patterns of the composite coatings. The diffraction peaks of the composite coating exhibit polycrystalline orientation. It can be seen from Figure 4a that the composite coating deposited at 0 g·L^{-1} MoS_2 contains Ni, Co and Al_2O_3, and the diffraction peaks of each phase are obvious. As seen in Figure 4b, the characteristic peaks of MoS_2 are also found at 2θ=14.533°, corresponding

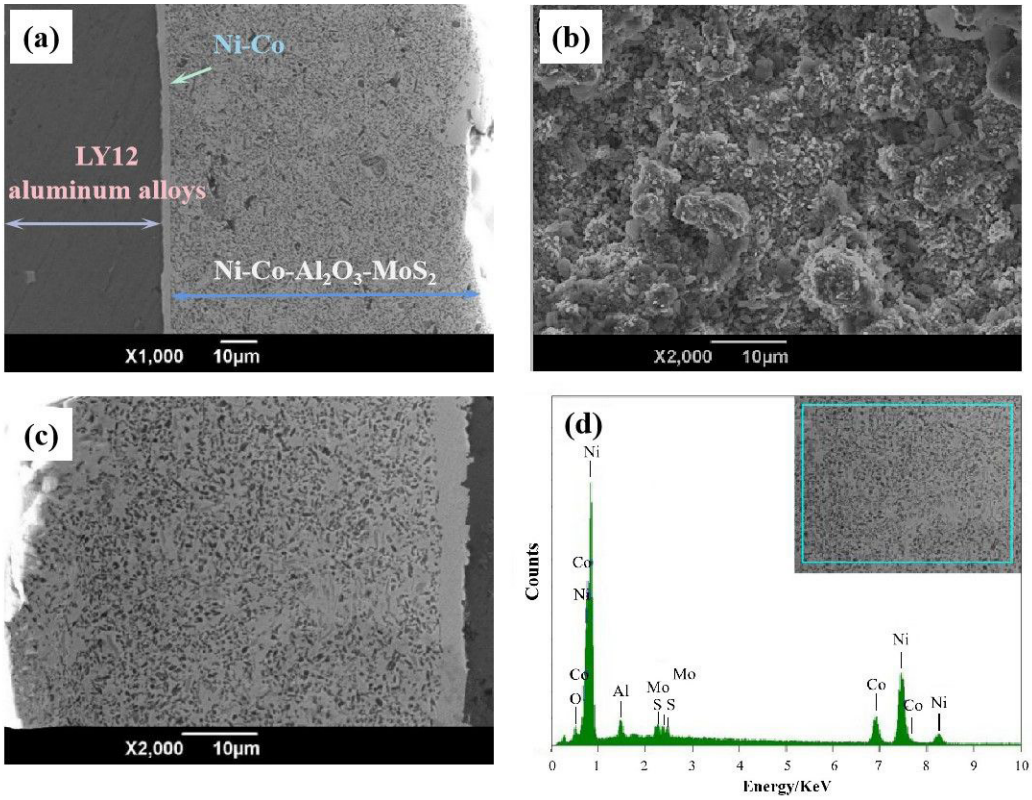

Figure 2. Composition and morphologies of as-prepared Ni-Co matrix composites.

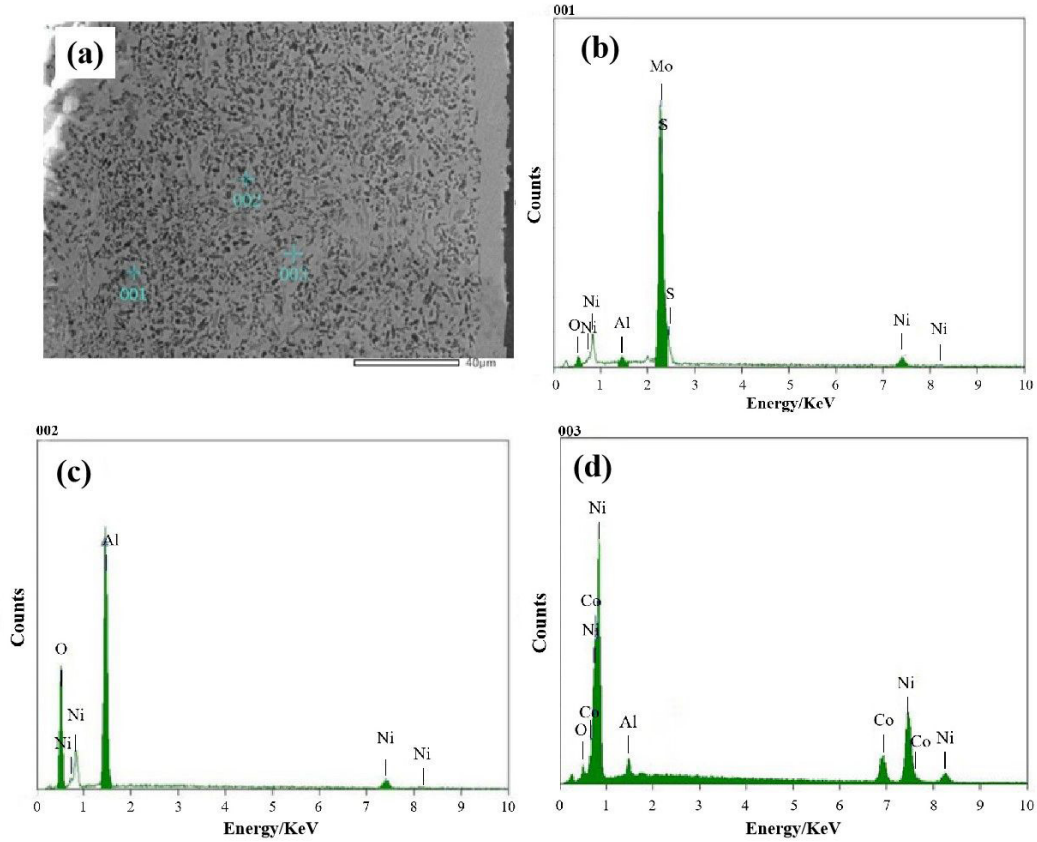

Figure 3. Energy spectrum of the as-deposited composites.

(002) plane. Therefore, the composite coating synthesized at 1.0 g·L^{-1} MoS_2 contains Ni, Co, Al_2O_3 and MoS_2.

Figure 5 shows the cross-section morphologies of the composite coatings synthesized at various MoS_2 concentrations. It can be seen from Figure 5 that the composite coating is well bonded with the substrate, and there is no crack and void at the interface. The average thickness of the Ni-Co intermediate layer is about 5.571 μm. By introducing 1.0 g·L^{-1} MoS_2 particles, the composite coating is dense and uniform, and the average thickness of the coating reached a minimum of 39.820 μm (Figure 5b). This may be attributed to the stable suspension of MoS_2 and Al_2O_3 particles in the bath, and then the suspended particles are uniformly deposited on the cathode surface, resulting in the uniform and dense microstructure of the coating. If the MoS_2 concentration is not optimal (1.0 g·L^{-1}), numerous pores appear in the composite coating. As seen in the Figure 5d, there are particularly large pores in the composite coating. Because MoS_2 particles are hydrophobic

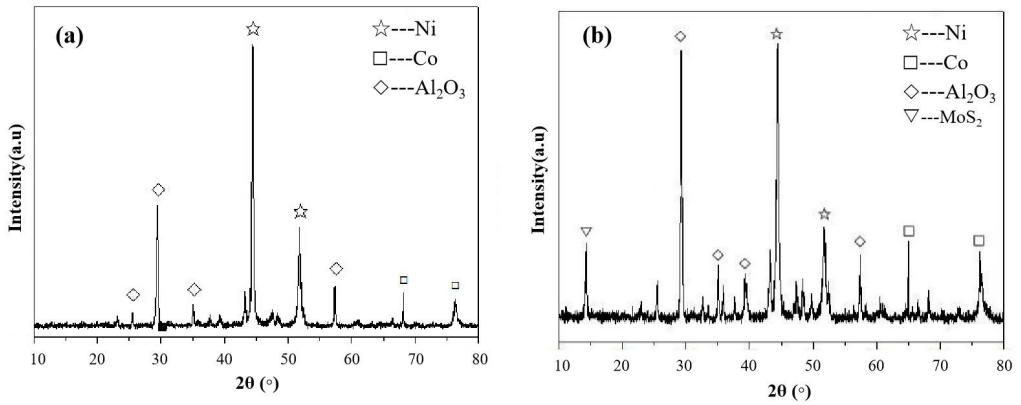

Figure 4. XRD patterns of the electrophoretic-electrodeposited composites: (a) without adding MoS_2, (b) adding 1.0 g·L^{-1} MoS_2.

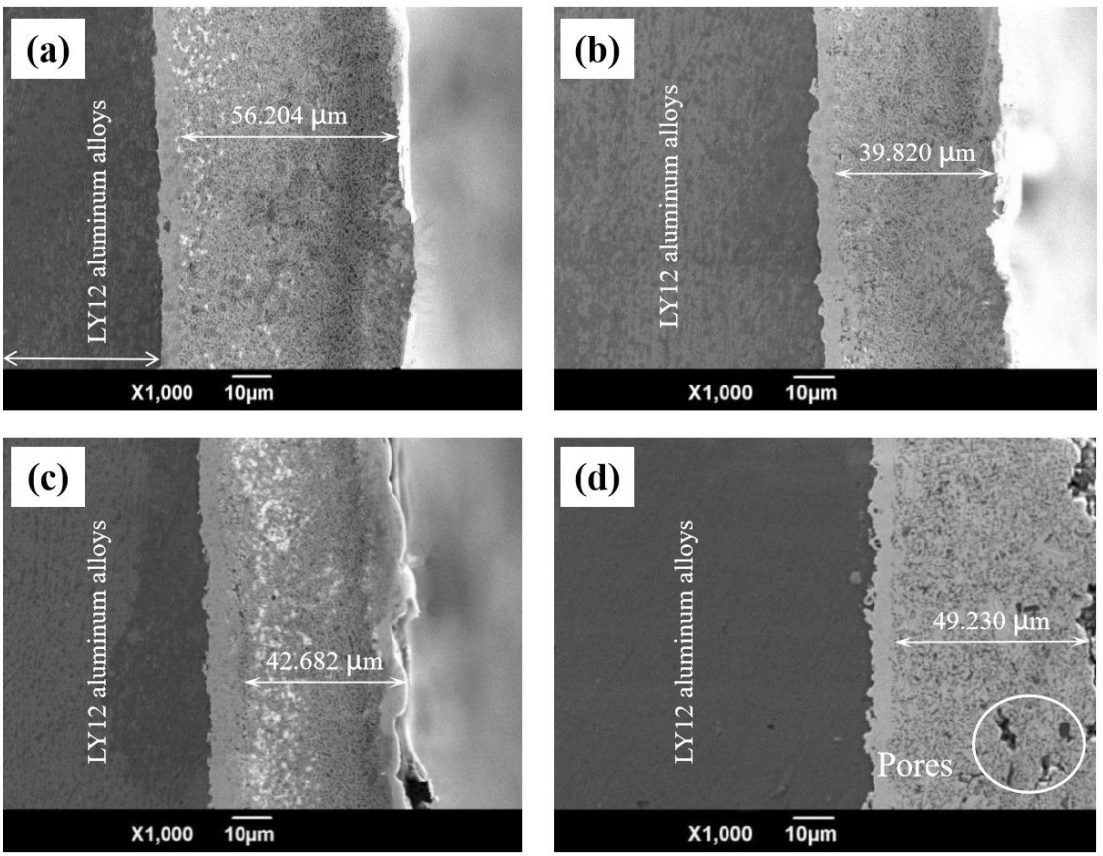

Figure 5. Cross-section morphologies of the coating with various MoS_2 concentrations: (a) 0.5 g·L^{-1}; (b) 1.0 g·L^{-1}; (c) 1.5 g·L^{-1}; (d) 2.0 g·L^{-1}.

and with a larger wetting angle in water, the hydrophobicity of MoS_2 particles directly affects the deposition of Ni-Co metal matrix. Ni-Co matrix could not completely fill the pores between the particles, which lead to a large number of pores in the coating.

Figure 6 presents the surface morphologies of as-synthesized Ni-Co-Al_2O_3-MoS_2 composites. As can be seen, with the increase of MoS_2 concentration to 1.0 g·L^{-1}, the composite coating with uniform, flat and fine surface morphology is observed (Figure 6b). The conductive MoS_2 particles adsorbed on the cathode surface increase the reaction area of nickel ions and cobalt ions and provide more nucleation sites during the pulse electrodeposition process, thus the coating surface presents a relatively smooth and dense morphology[28]. As shown in Figure 6c and Figure 6d, with the increase of MoS_2 concentration to 1.5 g·L^{-1} and 2.0 g·L^{-1} respectively, rough mushroom-like microstructure is formed on the coating surface. This is mainly due to the agglomeration of MoS_2 in the electrophoresis bath, and then the deposition of these aggregates on the cathode surface. During the subsequent pulse electrodeposition process, the applied current is more concentrated on the conductive particles, which leads to the priority reduction of Ni^{2+} and Co^{2+} on the raised aggregates. At the same time, because of the electric field repulsion between the protrusions, the reduction of metal ions in the grooves is hindered, which exacerbates the roughness of the composite coating and then forms a mushroom-like structure.

Table 2 tabulates the EDS results of Ni-Co-Al_2O_3-MoS_2 composite coatings. With the increase of MoS_2 concentration, the contents of Ni and Co in the composite coating are gradually decreased. When the MoS_2 concentration is low (< 1.0 g·L^{-1}), the relative contents of Al and O present an increasing trend. When the MoS_2 particles increased to 1.5 g·L^{-1} and 2.0 g·L^{-1}, the proportion of Al and O elements showed a downward trend, indicating that the introduction of MoS_2 particles inhibited the deposition of Al_2O_3 particles.

3.2 Micro-indentation hardness

The micro-indentation hardness of the Ni-Co-Al_2O_3-MoS_2 composites is provided in Figure 7. With increasing

Table 2. Results of energy spectrum analysis of the coatings.

MoS_2	Ni/at%	Co/at%	Al/at%	O/at%	Mo/at%	S/at%
0.5 g·L^{-1}	36.27	21.12	14.57	20.34	3.11	4.59
1.0 g·L^{-1}	35.96	20.66	15.80	19.88	4.66	5.04
1.5 g·L^{-1}	35.90	19.81	12.12	17.97	5.99	8.21
2.0 g·L^{-1}	35.17	19.72	12.25	16.91	6.09	9.86

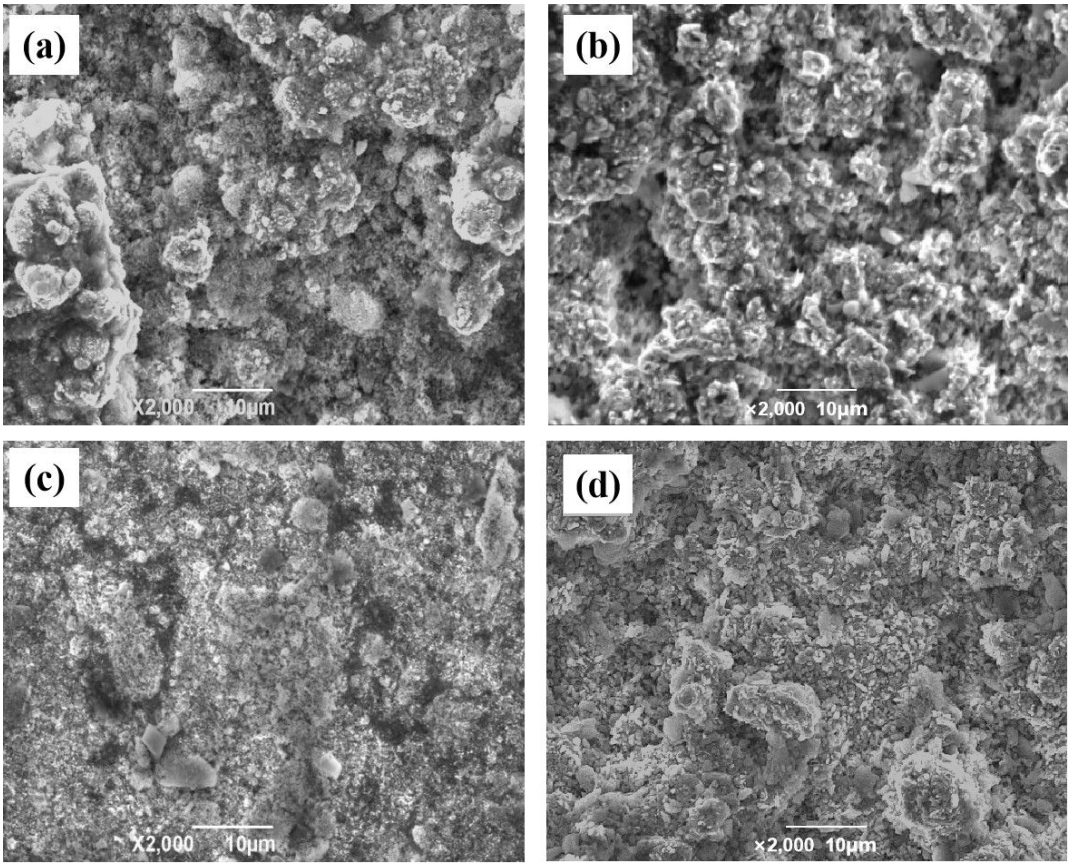

Figure 6. Surface morphologies of the composite coating with different MoS_2 addition: (a) 0.5 g·L^{-1}; (b) 1.0 g·L^{-1}; (c) 1.5 g·L^{-1}; (d) 2.0 g·L^{-1}.

the concentration of MoS_2 particles, the micro-indentation hardness of the composite coating tends to decrease. Due to introducing soft particles of MoS_2, the micro-indentation hardness of the composite coating is correspondingly reduced. In addition, the addition of MoS_2 hinders the deposition of Al_2O_3 particles and weakens the strengthening effect of hard particles in the coating, which is consistent with EDS results.

3.3 Friction and wear

It is generally considered that low friction coefficient and wear rate represent excellent friction and wear resistance. Figure 8 shows the friction coefficient of Ni-Co matrix composite coatings. It can be seen that the friction coefficient of the coating deposited at 1.0 g·L^{-1} MoS_2 reaches the lowest value, which indicates that the coating has excellent anti-friction performance. The micro-hardness of the composite coating without introduction of MoS_2 is higher because it has more Al_2O_3 particles. As the friction continues, the Al_2O_3 particles in the coating are gradually exposed and even fall off. The exfoliated Al_2O_3 particles act as abrasive particles in the process of wear, so that the original adhesive wear changes to abrasive wear, which further aggravates the wear[29]. Therefore, the friction coefficient increases quickly and then remains at a high level of friction balance in coefficient state. With the introduction of MoS_2 particles into the composite coating, the friction coefficient of the composite coating is lower than that without adding MoS_2 particles, which proves that MoS_2 plays a lubricating role to a certain extent. As the concentration of MoS_2 was increased to 1.0 g·L^{-1}, the composite coating became extremely smooth and dense, and the friction coefficient of the coating decreased significantly. This phenomenon may be attributed to the formation of lubricating film on the coating surface, which effectively improves the wear resistance of the coating[30]. If the MoS_2 concentration exceeds 1.0 g·L^{-1}, many bumps appear on the coating surface, and the surface quality of the coating deteriorates obviously. In addition, the uneven distribution of particles and the appearance of defects such as holes and cracks cause the coating structure to be extremely uneven, which leads to the increase of friction coefficient.

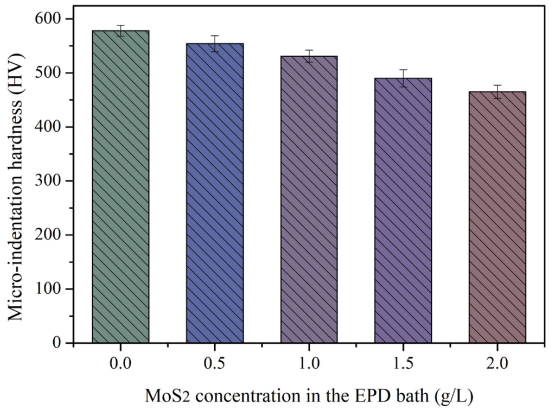

Figure 7. Micro-indentation hardness of the composite coatings.

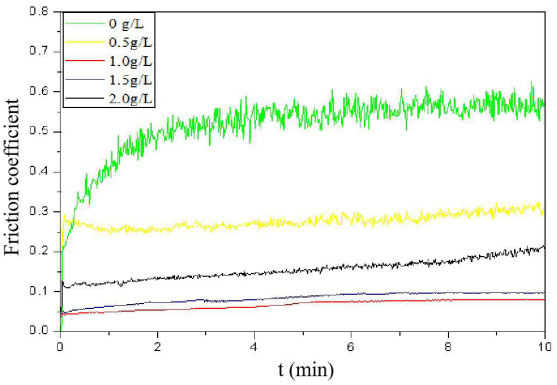

Figure 8. The effect of MoS_2 addition on the friction coefficient of the composite coating.

The schematic of the friction mechanism of the coating are shown in Figure 9. At the beginning of friction, MoS_2 particles are difficult to fully play the role of lubrication between friction pairs due to insufficient MoS_2 stripping. With the continuous friction and wear, a large number of MoS_2 particles are pulled out from the composite coating, forming a layer of self-lubricating film between the friction pairs, which significantly improves the wear resistance of Ni-Co-Al_2O_3-MoS_2 composite coatings. In addition, the uniformly distributed hard particles have "pinning effect" on the Ni-Co matrix, which effectively hinders the plastic deformation and exfoliation of the matrix during the process of friction and wear.

The wear rate of Ni-Co-Al_2O_3-MoS_2 composite coatings with various MoS_2 concentrations is presented in Figure 10. The minimum wear rate of the Ni-Co-Al_2O_3-MoS_2 composites fabricated at 1.0 g·L^{-1} MoS_2 is recorded, testifying the superior wear resistance. This is attributed to the uniform and dense

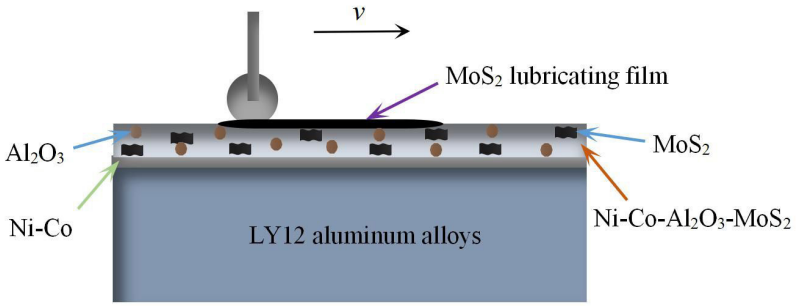

Figure 9. Schematic diagram of friction process of Ni-Co-Al_2O_3-MoS_2 composite coating prepared at 1.0 g·L^{-1} MoS_2.

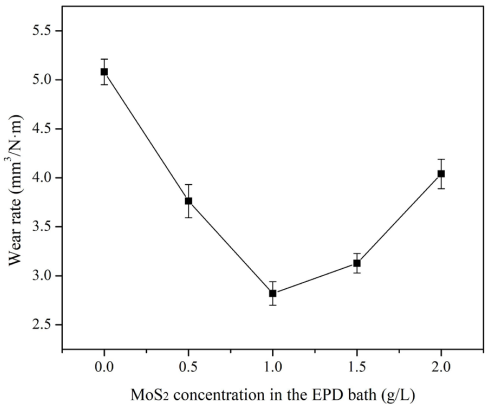

Figure 10. The variation of wear rate of the composite coatings prepared with different MoS_2 concentrations.

microstructure of the composite coating and the formation of solid lubricating film under this condition, which effectively alleviates the wear of the coating.

Figure 11 shows the worn scar morphologies of as-prepared composites. From Figure 11a concerning the worn scar morphology with 0 $g \cdot L^{-1}$ MoS_2, it can be seen that the wear is serious comparatively. Figure 11b shows a shallower mark than Figure 11a. MoS_2 particles, between the friction pairs, play a lubricating role to a certain extent. As the concentration of MoS_2 particles was increased to 1.0 $g \cdot L^{-1}$, a wide scratch appeared on the coating surface, and local peeling occurred due to adhesive wear (Figure 11c). This result seems to deviate from the low friction coefficient and wear rate. The reason may be due to the fact that the Ni-Co-Al_2O_3-MoS_2 composite coating fabricated at 1.0 $g \cdot L^{-1}$ MoS_2 is even and dense (confirmed by Figure 5b), and the protrusion

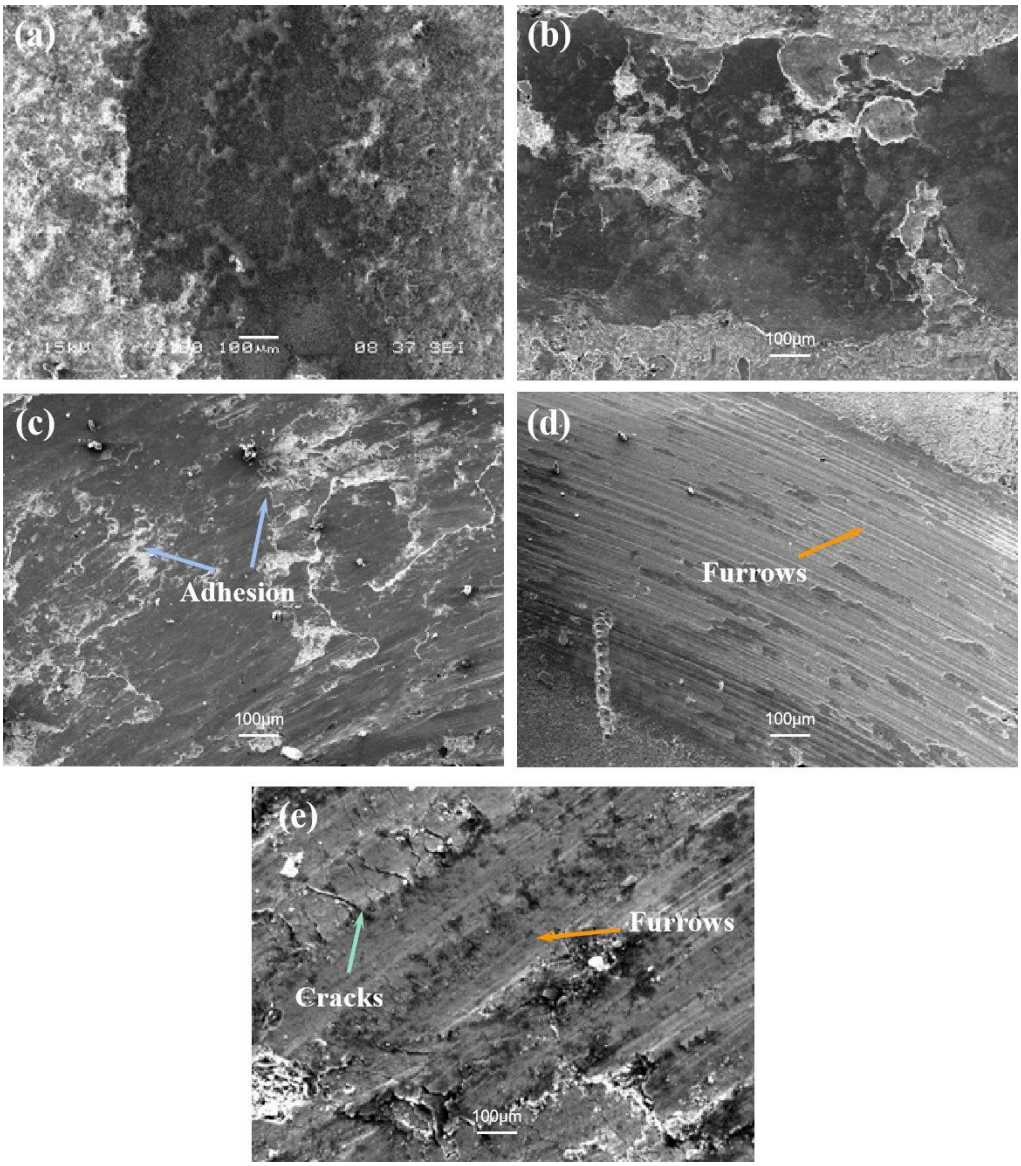

Figure 11. SEM images of worn morphology of as-fabricated composites: (a) without adding MoS_2 particles; (b) and (c) adhesive wear of the coatings with MoS_2 concentration of 0.5 $g \cdot L^{-1}$ and 1.0 $g \cdot L^{-1}$, respectively; (d) and (e) abrasive wear of the coatings with MoS_2 concentration of 1.5 $g \cdot L^{-1}$ and 2.0 $g \cdot L^{-1}$, respectively.

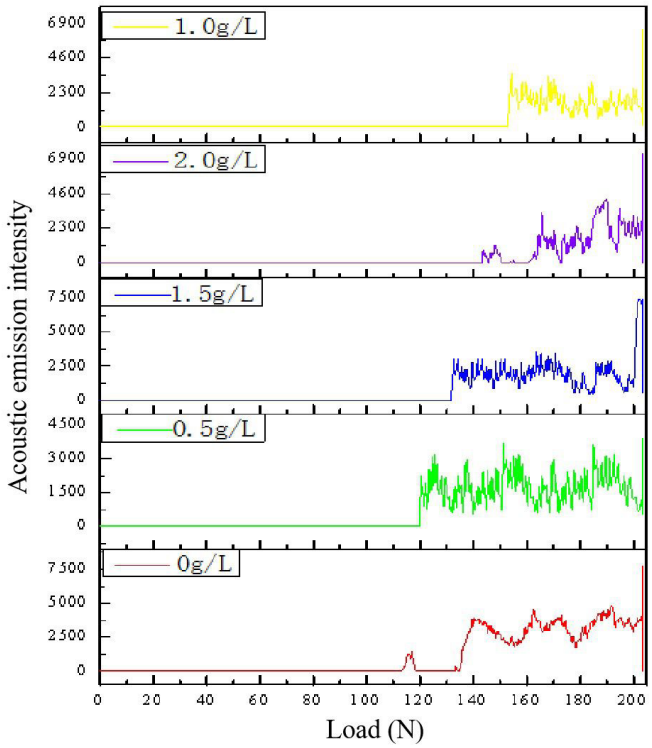

Figure 12. Acoustic emission spectra of Ni-Co matrix composite coatings.

formed on the coating surface is obviously reduced, thus losing the support function between the friction pairs, increasing the friction area, and finally leading to a wider wear mark. Simultaneously, the shortening of friction running in period because of the decrease of the protrusion and the formation of continuous lubricating film result in low friction coefficient and wear rate of the composite coating.

With the increase of MoS_2 concentration to 1.5 $g \cdot L^{-1}$, obvious furrows were observed by SEM (Figure 11d). This may be attributed to the uneven distribution of hard particles, and the agglomerated particles are prone to fall off. More abrasive particles are formed under the action of friction extrusion, which leads to serious abrasive wear on the coating surface. When the MoS_2 concentration is 2.0 $g \cdot L^{-1}$, many defects such as cracks and holes appear in the coating, which weakens the continuity and uniformity of the alloy matrix, and the coating surface becomes rough and uneven. During the process of friction and wear, a large number of cracks and furrows appear at the scratches, indicating severe wear conditions (Figure 11e).

3.4 The bonding force

The adhesion scratch test is designed to examine the bonding strength between coating and substrate. Figure 12 shows the curve of the acoustic emission signal-pressure loading (K-L) of the composite coatings. The acoustic emission spectrum is shown in red, corresponding to Ni-Co-Al_2O_3 composite coating. When the applied load reaches 117.8 N, the jumping increase of acoustic emission intensity indicates that the composite coating has failed. With the increase of MoS_2 concentration, the critical load initially increases and then decreases. The critical load of the composite coating containing 1.0 $g \cdot L^{-1}$ MoS_2 reaches the highest value about 154 N, which means that the Ni-Co matrix composite coating embedded with Al_2O_3 (10 $g \cdot L^{-1}$) and MoS_2 (1.0 $g \cdot L^{-1}$) has a good combination with LY12 aluminum alloy substrate.

4. Conclusions

1. Ni-Co matrix composites were successfully synthesized on the surface of LY12 aluminum alloys. At the MoS_2 concentration of 1.0 $g \cdot L^{-1}$, Ni-Co-Al_2O_3-MoS_2 composite coatings with uniform and compact microstructure were obtained, Al_2O_3 and MoS_2 particles were homogeneously embedded into the Ni-Co alloy matrix, and the average thickness of the coating was 39.820 μm. As the MoS_2 concentration was increased to 2.0 $g \cdot L^{-1}$, numerous defects such as holes and cracks appeared in the coating.
2. With the introduction of 1.0 $g \cdot L^{-1}$ MoS_2, the micro-indentation hardness of the coatings decreased slightly to 531 HV. In addition, the minimum friction coefficient and wear rate of the as-prepared composites were achieved at 1.0 $g \cdot L^{-1}$ MoS_2, which originated from the "pinning effect" of Al_2O_3 particles on Ni-Co matrix and the formation of a complete self-lubricating film. Meanwhile, the adhesion between the composite coating and the substrate was good, without obvious cracks and delamination. The maximum bonding strength was recorded as 154 N.

5. Acknowledgments

The work was supported by the National Natural Science Foundation of China (50172023) and the Shaanxi Industrial Science and Technology Research (2014K08-09) and the national college Students Innovation Training Program (202010704006).

6. References

1. Li XW, Zhang QX, Guo Z, Shi T, Yu JG, Tang MK, et al. Fabrication of superhydrophobic surface with improved corrosion inhibition on 6061 aluminum alloy substrate. Appl Surf Sci. 2015;342:76-83.
2. Egorkin VS, Gnedenkov SV, Sinebryukhov SL, Vyaliy IE, Gnedenkov AS, Chizhikov RG. Increasing thickness and protective properties of PEO-coatings on aluminum alloy. Surf Coat Tech. 2018;334:29-42.
3. Arboleda JA, Serna CM, Cadavid E, Barrios AC, Vargas F, Toro A. Effect of flame spray deposition parameters on the microstructure of Al_2O_3-13%TiO_2 coatings applied onto 7075 aluminum alloy. Mater Res. 2018;21(5)
4. Chen YM, Wang CT, Yang YC, Chen WJ. Application of aluminum-alloy mesh composite carbon cloth for the design of anode/cathode electrode s in Escherichia coli microbial fuel cell. Int J Hydrogen Energy. 2013;38(25):11131-7.
5. Li YX, Zhang PF, Bai PK, Wu LY, Liu B, Zhao ZY. Microstructure and properties of Ti/TiBCN coating on 7075 aluminum alloy by laser cladding. Surf Coat Tech. 2018;334:142-9.
6. Firouzdor V, Brechtl J, Hauch B, Sridharan K, Allen TR. Electrophoretic deposition of diffusion barrier titanium oxide coatings for nuclear reactor cladding applications. Appl Surf Sci. 2013;282:798-808.
7. Jafarpour M, Aghajani H. Electrophoretic deposition of bi-layered nano-sized silion carbide/mullite coating from stabilized suspensions. Journal of the Australian Ceramic Society. 2020;56(2):761-70.
8. Song G, Xu GQ, Quan YK, Yuan QC, Davies PA. Uniform design for the optimization of Al_2O_3 nanofilms produced by electrophoretic deposition. Surf Coat Tech. 2016;286:268-78.
9. Prado LH, Virtanen S. Cu-MoS_2 superhydrophobic coating by composite electrodeposition. Coatings. 2020;10(3):238.
10. Ma M, Sun WC, Zhang YG, Liu XJ, Dong YR, Zi JY, et al. Effect of TiC particles concentration on microstructure and properties of Ni-TiC composite coatings. Mater Res. 2020;22(6):e20190530.
11. Santillán MJ, Membrives F, Quaranta N, Boccaccini AR. Characterization of TiO_2 nanoparticle suspensions for electrophoretic deposition. J Nanopart Res. 2007;10(5):787-93.
12. Miao L, Cai S, Xiao Z. Preparation and characterization of nanostructured ZnO thin film by electrophoretic deposition from ZnO colloidal suspensions. J Alloys Compd. 2010;490(1-2):422-6.
13. Duan SC, Zhu DM, Zhou WC, Luo F, Chen Q. Mechanical and microwave absorption properties of SiC_f/SiC-Al_4C_3 composite with EPD-SiO_2/ZrO_2 interphase prepared by precursor infiltration and active filler-controlled pyrolysis method. Ceram Int. 2020;46(8):12344-52.
14. Jafarpour M, Aghajani H. Electrophoretic deposition of bi-layered nano-sized silicon carbide/mullite coating from stabilized suspensions. Journal of the Australian Society. 2020;56(2):761-70.
15. Cheng Q, Yao ZJ, Zhang F, Zhang SS, Oleksander M. Microstructure and tribological property of Ni-MoS_2 composite coatings prepared by ultrasonic and mechanical stirring. Mater Res Express. 2019;6(12):126434.
16. Guler ES, Konca E, Karakaya I. Investigation of the tribological behaviour of electrocodeposited Ni-MoS_2 composite coatings. Int J Surface Sci Eng. 2017;11(5):418-32.
17. He Y, Wang SC, Walsh FC, Chiu YL, Reed PAS. Self-lubricating Ni-P-MoS_2 composite coatings. Surf Coat Tech. 2016;307:926-34.
18. Toosinezhad A, Alinezhadfar M, Mahdavi S. Tribological behavior of cobalt/graphene composite coatings. Ceram Int. 2020;46(10):16886-94.
19. Lupi C, Dell'Era A, Pasquali M, Imperatori P. Composition, morphology, structural aspects and electrochemical properties of Ni-Co alloy coatings. Surf Coat Tech. 2011;205(23-24):5394-9.
20. Elkhoshkhany N, Hafnway A, Khaled A. Electrodeposition and corrosion behavior of nano-structured Ni-WC and Ni-Co-WC composite coating. J Alloys Compd. 2017;695:1505-14.
21. Wang YY, Zhou XY, Liang ZP, Jin H. Characterization of ultrasonic-assisted electrochemical deposition of Ni-Co-ZrO_2. Coatings. 2018;8(6):211.
22. Hefnawy A, Elkhoshkhany N, Essam A. Ni-TiN and Ni-Co-TiN composite coatings for corrosion protection: fabrication and electrochemical characterization. J Alloys Compd. 2017;735:600-6.
23. Ma CY, Zhao DD, Ma ZP. Effects of duty cycle and pulse frequency on microstructures and properties of electrodeposited Ni-Co-SiC nanocoatings. Ceram Int. 2020;46(8):12128-37.
24. Li BS, Zhang WW. Synthesis and properties of a novel Ni-Co and Ni-Co/ZrO_2 composite coating by DC electrodeposition. J Alloys Compd. 2020;821:153258.
25. Jia ZW, Sun WC, Guo F, Dong YR, Liu XJ. Microstructure, friction and corrosion resistance properties of a Ni-Co-Al_2O_3 composite coating. RSC Advances. 2018;8(22):12138-45.
26. Wang Y, Sun WC, Wang CA, Huang Y, Xu JM. Microstructure, friction, and wear properties of Ni-Al_2O_3-MoS_2 composite coatings. Int J Appl Ceram Technol. 2017;14(5):889-98.
27. Li BS, Zhang WW. Synthesis of Ni-Co-ZrO_2 nanocomposites doped with ceria particles via electrodeposition as highly protective coating. J Alloys Compd. 2020;820:153158.
28. Xia FF, Li Q, Ma CY, Liu WQ, Ma ZP. Preparation and wear properties of Ni/TiN–SiC nanocoatings obtained by pulse current electrodeposition. Ceram Int. 2020;46(6):7961-9.
29. Sun WC, Zhang P, Zhao K, Tian MM, Wang Y. Effect of graphite concentration on the friction and wear of Ni-Al_2O_3/graphite composite coatings by a combination of electrophoresis and electrodeposition. Wear. 2015;342:172-80.
30. Zhang YY, Epshteyn Y, Chromik RR. Dry sliding wear behaviour of cold-sprayed Cu-MoS_2 and Cu-MoS_2-WC composite coatings: the influence of WC. Tribol Int. 2018;123:296-306.